

Forward-Flyback Converter with Current-Doubler Rectifier: Analysis, Design, and Evaluation Results

Laszlo Huber, *Member, IEEE*, and Milan M. Jovanović, *Senior Member, IEEE*

Abstract—Complete design-oriented steady-state analysis of the forward-flyback converter with the current-doubler rectifier is provided. Advantages and disadvantages of this topology compared to the conventional forward converter are discussed. In particular, the transformer-secondary copper losses are evaluated. In addition, a step-by-step design procedure is given. Finally, experimental evaluation results obtained on a 3.3-V/50-A dc/dc converter prototype for the 40–60-V input-voltage range are presented.

Index Terms—Current-doubler rectifier, dc–dc power conversion, forward-flyback converter, HF transformer winding loss.

I. INTRODUCTION

IN A CONTINUING effort to decrease power consumption and increase the speed of data-processing circuits, their power-supply-voltage requirements are continuously being reduced. Currently, 3.3-V integrated circuits (IC's) are gradually replacing the standard 5-V IC's due to their better speed/power-consumption performance and higher integration densities. However, the transition to lower supply voltages usually requires higher output currents as well as lower output-voltage ripples. As a result, the design of an efficient secondary-side circuit is an extremely challenging task. The efficiency of the secondary-side circuit in a converter with a high-output current may be improved by employing the current-doubler-rectifier (CDR), also called hybrid, technique. The idea was first described in [1], while implementations of the CDR in the half-bridge, full-bridge, and forward converters were reported in [2]–[7]. Since the forward converter with CDR operates in a forward-flyback fashion, this topology is more appropriately called forward-flyback converter with CDR. The CDR offers the following advantages compared to the conventional secondary-side rectifier topologies such as the full-wave diode bridge, full-wave rectifier with center-tapped transformer secondary, and conventional forward:

- 1) reduced rms value of the transformer-secondary current;
- 2) reduced output-voltage ripple through cancellation of ripple currents of the two output inductors;
- 3) extended continuous-conduction-mode (CCM) range to lower output currents;
- 4) more evenly distributed power dissipation.

Manuscript received September 18, 1997; revised June 17, 1998. Recommended by Associate Editor, O. Mandhana.

The authors are with the Delta Products Corporation, Power Electronics Laboratory, Research Triangle Park, NC 27709 USA (e-mail: lhuber@deltartp.com).

Publisher Item Identifier S 0885-8993(99)00297-5.

This paper provides a complete steady-state analysis of the forward-flyback converter with CDR. To facilitate the understanding of operation, the converter circuit in each topological stage within a switching cycle is reduced to a first- or second-order equivalent circuit. Design guidelines are also given. Advantages and disadvantages of the CDR forward-flyback converter versus the conventional forward converter are evaluated on a 3.3-V/50-A dc/dc converter prototype for the 40–60-V input-voltage range. In particular, the transformer-secondary copper losses are carefully evaluated.

II. ANALYSIS

The circuit diagram of the active-clamp forward-flyback converter with the current-doubler rectifier is shown in Fig. 1. There are two possible CDR topologies: with common-anode diodes [Fig. 1(a)] and with common-cathode diodes [Fig. 1(b)]. For practical implementation, the CDR with common-cathode diodes is more convenient due to the widespread availability of the common-cathode configuration in a single package. To simplify the analysis, output filter inductances L_1 and L_2 and clamp capacitance C_{cl} are assumed to be sufficiently large. Thus, they can be considered as current and voltage sources, as shown in the equivalent circuit in Fig. 2. Also, it is assumed that all semiconductor components are ideal, except for the output capacitances of switches Q_1 and Q_2 , which are included into equivalent parallel capacitance C_{eq} . The magnetizing current i_M of the transformer consists of dc component $I_M = I_o/(2N)$, which is necessary to support the secondary current during off time and ac component i_m . Inductances L_{lkp} and L_{lks} are the primary- and secondary-side leakage inductances.

Under steady-state operation, eight stages can be identified within each switching cycle, as shown in Fig. 3. Key waveforms are presented in Fig. 4. For clarity, the durations of the turn-on and turn-off intervals are exaggerated.

During $[T_0 - T_1]$ interval, switch Q_1 is on and its current is equal to the sum of reflected secondary current $I_o/2N$ and magnetizing current i_M , which increases with a constant slope V_i/L_m , i.e.,

$$\begin{aligned} i_{Q1} &= \frac{I_o}{2N} + I_M + i_m \\ &= \frac{I_o}{N} + i_m(T_0) + \frac{V_i}{L_m} \cdot (t - T_0). \end{aligned} \quad (1)$$

The whole output current flows through diode D_1 , as shown in Fig. 3.

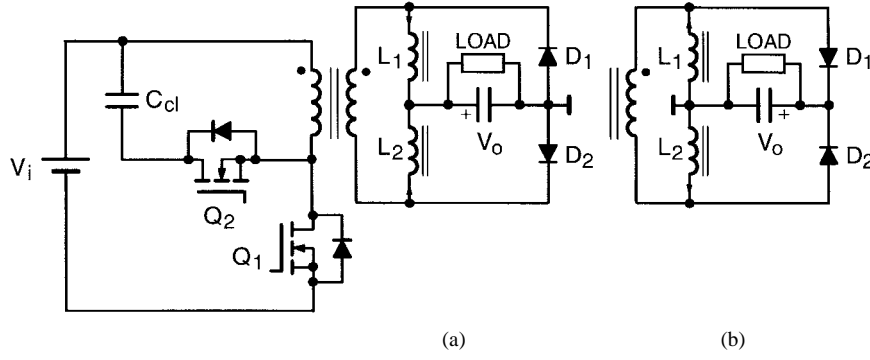


Fig. 1. Circuit diagram of active-clamp forward-flyback converter with CDR: (a) common-anode diodes and (b) common-cathode diodes.

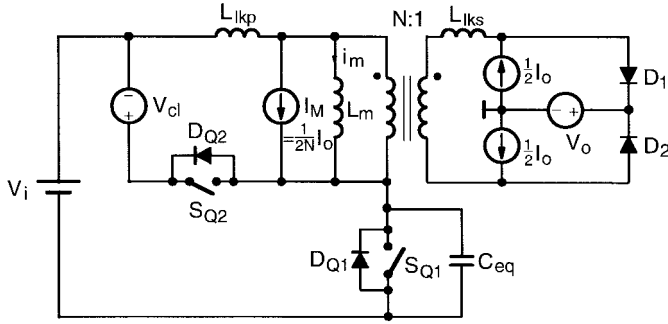


Fig. 2. Equivalent circuit of active-clamp forward-flyback converter with CDR.

Switch Q_1 is turned off at $t = T_1$. During $[T_1-T_2]$ interval, capacitance C_{eq} is almost linearly charged from zero voltage to input voltage V_i by an approximately constant current

$$i_{Ceq} \approx \frac{I_o}{N} + i_m(T_1). \quad (2)$$

At $t = T_2$, secondary voltage v_S reaches zero and diode D_2 starts to conduct. During commutation of the output current from D_1 to D_2 and vice versa, leakage inductances L_{lkp} and L_{lks} play a significant role.

During $[T_2-T_3]$, inductances L_{lkp} and L_{lks} resonate with capacitance C_{eq} , as shown in the equivalent subcircuit in Fig. 5(a). It can be assumed that during commutation of the output current from D_1 to D_2 , the magnetizing current is approximately constant and equal to its maximum value

$$i_M \approx i_M^{\max} = \frac{I_o}{2N} + \frac{\Delta i_M}{2} \quad (3)$$

where Δi_M is the peak-to-peak variation of the magnetizing current. The constant magnetizing current flowing through leakage inductance L_{lkp} does not cause an additional voltage drop on L_{lkp} , and, therefore, the subcircuit in Fig. 5(a) can be simplified as shown in Fig. 5(b). Notice that the current of the total equivalent leakage inductance i_{Llk} is equal to the reflected secondary current i_S/N . Current i_{Llk} decreases in a resonant fashion

$$i_{Llk} = -\left(\frac{I_o}{2N} + \frac{\Delta i_M}{2}\right) + \left(\frac{I_o}{N} + \frac{\Delta i_M}{2}\right) \cdot \cos(\omega_r(t - T_2)) \quad (4)$$

where

$$\omega_r = \frac{1}{\sqrt{L_{lk}C_{eq}}} \quad (5)$$

is the angular resonant frequency. The voltage on C_{eq} during $[T_2-T_3]$ increases as

$$v_{Ceq} = V_i + V_r^+ \cdot \sin(\omega_r(t - T_2)) \quad (6)$$

where the amplitude of the sinusoidal component is

$$V_r^+ = Z_r \cdot \left(\frac{I_o}{N} + \frac{\Delta i_M}{2}\right) \quad (7)$$

and

$$Z_r = \sqrt{\frac{L_{lk}}{C_{eq}}} \quad (8)$$

is the characteristic impedance of the resonant circuit in Fig. 5(b). Interval $[T_2-T_3]$ terminates either when voltage v_{Ceq} rises to $V_i + V_{cl}$ and clamp diode D_{Q2} starts to conduct or when the output current completely commutates from D_1 to D_2 and diode D_1 turns off, whichever occurs first. Notice that for $i_{D2} = I_o$, $i_{Llk} = -I_o/(2N)$ is necessary. In Fig. 4, it is assumed that voltage v_{Ceq} reaches $V_i + V_{cl}$ before diode D_2 takes the full output current. The condition for this can be obtained from (4) and (6) as

$$\sqrt{1 - \left(\frac{V_{cl}}{V_r^+}\right)^2} > \frac{\frac{\Delta i_M}{2}}{\frac{I_o}{N} + \frac{\Delta i_M}{2}}. \quad (9)$$

For example, when $\Delta i_M/2 = I_o/(2N)$, as in Fig. 4, it follows from (9) that $V_{cl} < 0.94 \cdot V_r^+$.

During $[T_3-T_5]$ interval, the voltage on C_{eq} is clamped to $V_i + V_{cl}$. Using the same reasoning as during $[T_2-T_3]$ interval, the equivalent subcircuit during $[T_3-T_5]$ interval is obtained as shown in Fig. 5(c). Leakage-inductance current i_{Llk} decreases with a constant slope $-V_{cl}/L_{lk}$. At $t = T_4$, secondary current i_S changes sign. At $t = T_5$, diode current i_{D2} reaches the full output current and diode D_1 turns off.

If during $[T_2-T_3]$ interval the commutation of the output current from D_1 to D_2 completes before voltage v_{Ceq} reaches $V_i + V_{cl}$, then during $[T_3-T_5]$ interval, capacitor C_{eq} will continue to be charged by the ac component of the magnetizing current $i_m = \Delta i_M/2$ as the entire dc component I_M is needed to support negative secondary current $i_S = -I_o/2$. In this

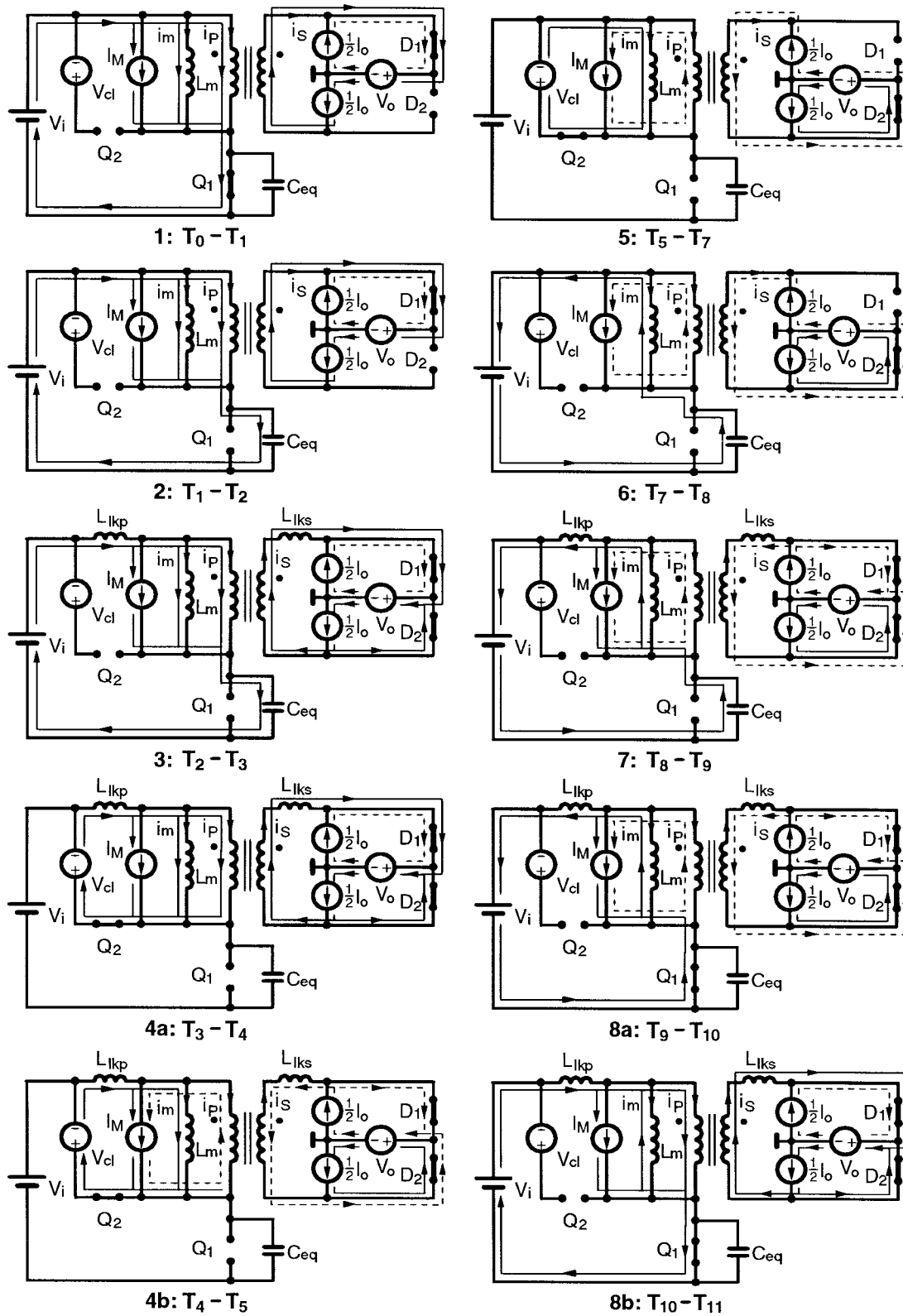


Fig. 3. Equivalent topological stages.

case, voltage v_{Ceq} reaches $V_i + V_{cl}$ and diode D_{Q2} starts to conduct at $t = T_5$.

During $[T_5-T_7]$ interval, dc magnetizing current I_M supports negative secondary current $i_S = -I_o/2$ and ac magnetizing current i_m flows through clamp-voltage source V_{cl}

decreasing with a constant slope $-V_{cl}/L_m$. During $[T_5-T_6]$, i_m is positive and flows through diode D_{Q2} , and during $[T_6-T_7]$, i_m is negative and flows through switch S_{Q2} . Switch S_{Q2} should be turned on during $[T_5-T_6]$ interval to assure turn on with zero voltage.

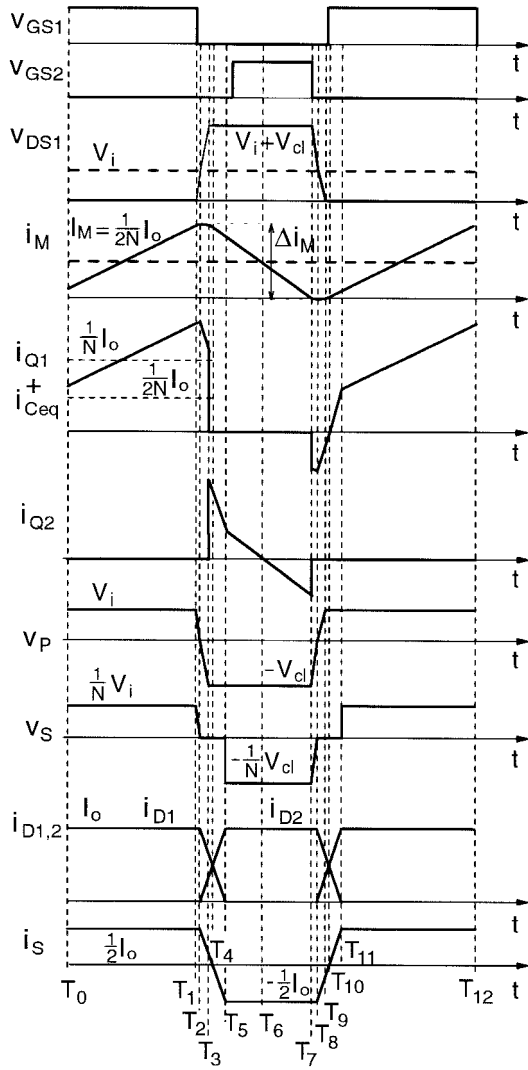


Fig. 4. Key waveforms.

At $t = T_7$, switch S_{Q2} is turned off and ac magnetizing current i_m is commutated from switch S_{Q2} to capacitance C_{eq} . During $[T_7-T_8]$ interval, capacitance C_{eq} is almost linearly discharged from voltage $V_i + V_{cl}$ to input voltage V_i by the ac magnetizing current, which can be approximated as constant during $[T_7-T_8]$, i.e.,

$$i_{Ceq} = i_m \approx i_m(T_7). \quad (10)$$

At $t = T_8$, secondary voltage v_s reaches zero and diode D_1 starts to conduct. During commutation of the output current from D_2 to D_1 , the magnetizing current is approximately constant and equal to its minimum value

$$i_M \approx i_M^{\min} = \frac{I_o}{2N} - \frac{\Delta i_M}{2}. \quad (11)$$

Using again the same reasoning as during $[T_2-T_3]$ interval, the equivalent subcircuit during $[T_8-T_9]$ interval is obtained as shown in Fig. 5(d). The equivalent leakage inductance on the primary side of the transformer L_{lk} resonates with capacitance C_{eq} . Current i_{Llk} , which is equal to reflected secondary current

i_S/N , and current i_{Ceq} increase in a resonant fashion

$$i_{Llk} = -\frac{I_o}{2N} + \frac{\Delta i_M}{2} - \frac{\Delta i_M}{2} \cdot \cos(\omega_r(t - T_8)) \quad (12)$$

and

$$i_{Ceq} = -\frac{\Delta i_M}{2} \cdot \cos(\omega_r(t - T_8)). \quad (13)$$

The voltage on C_{eq} during $[T_8-T_9]$ decreases as

$$v_{Ceq} = V_i - V_r^- \cdot \sin(\omega_r(t - T_8)) \quad (14)$$

where

$$V_r^- = Z_r \cdot \frac{\Delta i_M}{2}. \quad (15)$$

Interval $[T_8-T_9]$ terminates either when voltage v_{Ceq} decreases to zero and diode D_{Q1} starts to conduct or when the output current completely commutates from D_2 to D_1 and diode D_2 turns off, whichever occurs first. In Fig. 4, it is assumed that voltage v_{Ceq} decreases to zero before diode D_1 takes the full output current. The condition for this can be obtained from (12) and (14) as

$$\sqrt{1 - \left(\frac{V_i}{V_r^-}\right)^2} > \frac{-\frac{I_o}{N} + \frac{\Delta i_M}{2}}{\frac{\Delta i_M}{2}}. \quad (16)$$

For all cases when $\Delta i_M/2 < I_o/N$, which also includes the example in Fig. 4 [$\Delta i_M/2 = I_o/(2N)$], the only condition required to satisfy (16) is $V_i < V_r^-$.

During $[T_9-T_{11}]$ interval, the voltage on C_{eq} is equal to zero. Using the same reasoning as during $[T_2-T_3]$ interval, the equivalent subcircuit during $[T_9-T_{11}]$ interval is obtained as shown in Fig. 5(e). Leakage-inductance current i_{Llk} and switch current i_{Q1} increase with a constant slope V_i/L_{lk} .

During $[T_9-T_{10}]$ interval, current i_{Q1} is negative and flows through diode D_{Q1} . Switch S_{Q1} should be turned on during this interval; that results in turn on at zero voltage or zero-voltage switching (ZVS). During $[T_{10}-T_{11}]$ interval, current i_{Q1} is positive, and it flows through switch S_{Q1} . At $t = T_{11}$, diode current i_{D1} reaches the full output current and diode D_2 turns off, starting the next switching cycle.

III. DESIGN

The design of the forward-flyback converter with CDR is illustrated on a 3.3-V/50-A dc/dc converter for the 40–60-V input-voltage range. The key design parameters are the minimum and maximum duty cycles D_{\min} and D_{\max} , turns ratio of the transformer N , switching frequency f_S , and air-gap length l_g of the selected transformer core.

The output voltage of the CDR forward-flyback converter in continuous conduction mode (CCM) of operation is determined by the same expression as the output voltage of the conventional forward converter in CCM

$$V_o = D \cdot \frac{V_i}{N} - V_F \quad (17)$$

where V_F is the forward-voltage drop on the secondary-side diodes. From (17), the ratio of the maximum and minimum

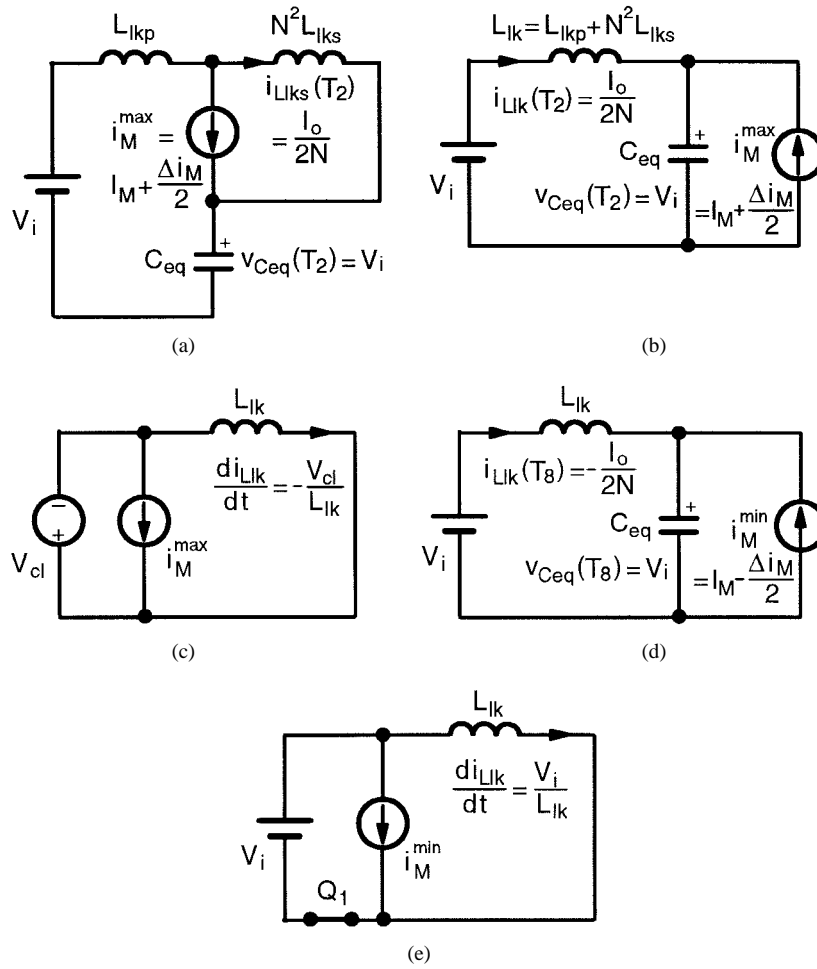


Fig. 5. Equivalent primary-side subcircuit during (a) and (b) $[T_2-T_3]$, (c) $[T_3-T_5]$, (d) $[T_8-T_9]$, and (e) $[T_9-T_{11}]$ intervals.

duty cycles is obtained as

$$\frac{D_{\max}}{D_{\min}} = \frac{V_{i \max}}{V_{i \min}} = 1.5. \quad (18)$$

The conventional design approach of the active-clamp forward converter is to minimize the switch voltage stress over the input voltage range, i.e., to ensure equal switch voltage stress at minimum and maximum input voltages. The voltage stress on both switches Q_1 and Q_2 in Fig. 1 is equal to $V_i + V_{cl}$. The clamp voltage is obtained from the flux balance of the transformer

$$V_{cl} = \frac{D}{1-D} \cdot V_i. \quad (19)$$

Using (19), the voltage stress on both switches is

$$V_{Q \max} = \frac{V_i}{1-D}. \quad (20)$$

The condition for equal switch-voltage stresses at minimum and maximum input voltages is obtained from (18) and (20) as

$$D_{\max} + D_{\min} = 1. \quad (21)$$

It follows from (18) and (21) that $D_{\min} = 0.4$ and $D_{\max} = 0.6$. Then, from (17), the transformer turns ratio $N = 6.6 \approx 7$ is obtained, where $V_F = 0.35$ V was used. Substituting

back in (17), the corrected minimum and maximum duty cycles are $D_{\min} = 0.43$ and $D_{\max} = 0.64$. From (20), the switch voltage stresses are $V_Q(V_{i \min}) = 110.7$ V and $V_Q(V_{i \max}) = 104.5$ V. For the switches, 200-V MOSFET's were selected as shown in Fig. 6. The voltage stresses on the secondary-side diodes are

$$V_{D1 \max} = \frac{V_{cl \max}}{N} - V_F = 9.8 \text{ V} \quad (22)$$

and

$$V_{D2 \max} = \frac{V_{i \max}}{N} - V_F = 8.2 \text{ V}. \quad (23)$$

For secondary-side diodes, 15-V Schottky diodes—which have the lowest forward-voltage drop—can be employed.

Using Faraday's law and (17), the transformer-flux excursion is obtained as

$$\Delta B = \frac{V_o + V_F}{N_S A_c f_S} \quad (24)$$

where N_S is the number of secondary turns and A_c is the effective cross-sectional area of the transformer core. To minimize the transformer-secondary copper loss, $N_S = 1$ is selected. Choosing the switching frequency $f_S = 250$ kHz and selecting the economic-flat-design core EFD30-3F3 [8], $\Delta B = 212$ mT is obtained.

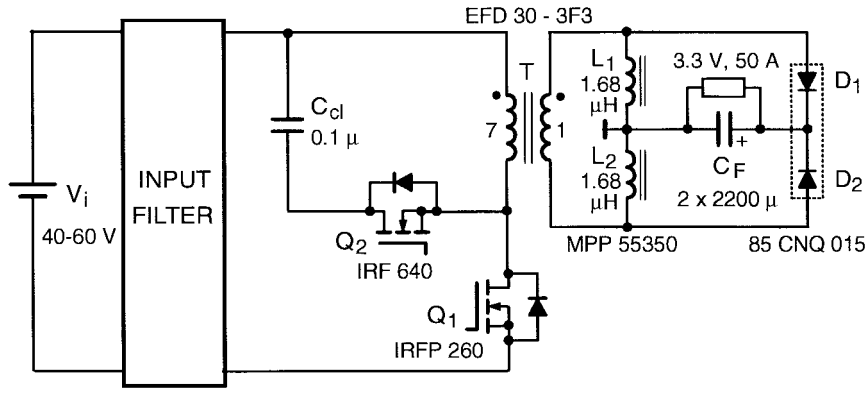


Fig. 6. Experimental circuit diagram.

The air-gap length is determined from the required stored energy in the transformer. Choosing $B_{\max} = \Delta B$ (see Fig. 4), the stored energy in the transformer is

$$W_c = \frac{A_c \cdot B_{\max}^2}{2\mu_o} \left(l_g + \frac{l_c}{\mu_a} \right) = \frac{V_o I_o \max}{2\eta_{\min} f S} \quad (25)$$

where l_c is the effective core length, μ_a is the amplitude permeability, and η_{\min} is the estimated minimum efficiency. With $\eta_{\min} = 0.85$, from (25), the air-gap length $l_g = 0.3$ mm = 12 mil is obtained. The transformer primary and secondary windings are implemented with two strands of 150/42 Litz wire and two strands of 5-mil copper foil, respectively.

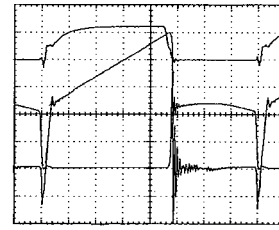
Each of the secondary-side inductors L_1 and L_2 is implemented with one molypermalloy powder (MPP) core 55 350 and four turns, four strands of wire AWG 17, resulting in $L_1 = L_2 = 1.68$ μ H.

The control circuit is based on the conventional low-cost current-mode pulsewidth modulation (PWM) controller integrated circuit (IC) 3843.

IV. EXPERIMENTAL RESULTS

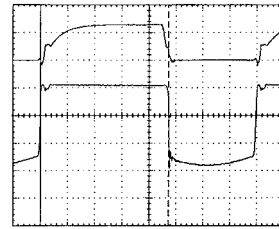
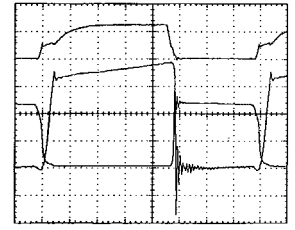
For experimental evaluation of the forward-flyback converter with CDR versus the conventional forward converter, the circuit shown in Fig. 6 was built. For the conventional forward converter, the same circuit was used, only the output filter inductor and the transformer gap were different: the output filter inductor was implemented with one MPP core 55930—which has about the same volume and weight as the two cores used in the forward-flyback converter with CDR—and three turns, six strands of wire AWG 17, resulting in 1.41- μ H inductance; the transformer gap was reduced to zero. Comparative experimental waveforms of the main-switch voltages and currents as well as of the transformer primary and secondary voltages at nominal input voltage ($V_i = 48$ V) and full load ($I_o = 50$ A) are shown in Fig. 7. As can be seen, the corresponding waveforms of the CDR forward-flyback and conventional forward converters are very similar, except for the main-switch current waveform i_{Q1} . The switch current of the CDR forward-flyback converter is significantly steeper during on time. In fact, the transformer of the CDR forward-flyback converter has a significantly lower magnetizing inductance in order to generate the dc

Forward-flyback with CDR

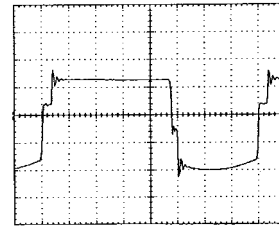
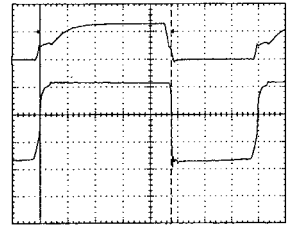


(a)

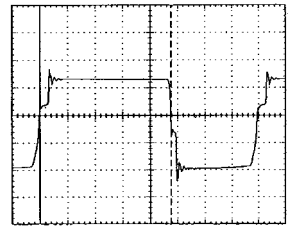
Conventional forward



(b)



500 ns/div



500 ns/div

(c)

Fig. 7. Experimental waveforms of (a) main-switch voltages and current, (b) transformer primary voltage, and (c) transformer secondary voltage at nominal input voltage ($V_i = 48$ V) and full load ($I_o = 50$ A).

magnetizing current needed to support the secondary current during off time. The switch voltage and current waveforms of the CDR forward-flyback converter in Fig. 7(a) nicely illustrate the ZVS at turn on. It should be noticed that the secondary voltage in Fig. 7(c) is different from zero during the output-current commutation intervals. This is caused by the additional voltage drop on the series inductances of diodes D_1 and D_2 , which was neglected in the analysis in Section II. In fact, the series inductances of the secondary-side diodes

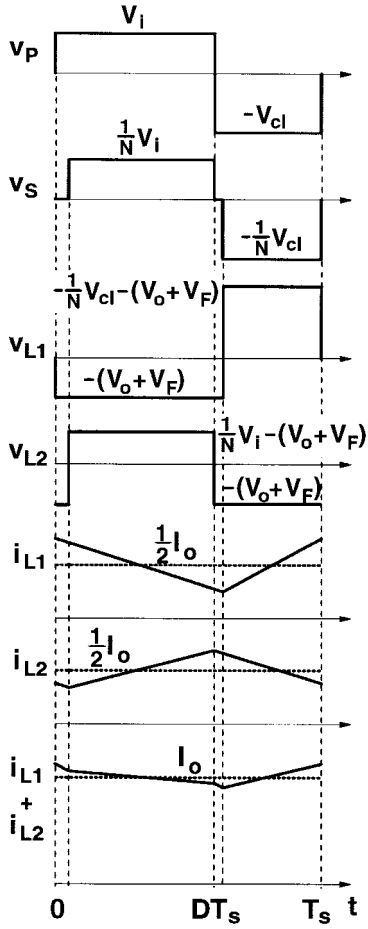


Fig. 8. Ripple cancellation.

increase the commutation time of the output current between the two diodes.

V. EVALUATION

The most important advantages of the CDR forward-flyback converter versus the conventional forward converter are:

- 1) smaller transformer-secondary copper loss;
- 2) smaller main-switch turn-on loss due to ZVS;
- 3) ripple cancellation seen by the output filter capacitor and secondary-side diodes (see Fig. 8).

The disadvantages of the CDR forward-flyback converter are:

- 1) larger transformer-primary copper loss;
- 2) larger transformer-core loss;
- 3) larger conduction loss of both switches;
- 4) larger turn-off loss of both switches.

Whether the advantages will prevail over the disadvantages depends on the input and output conditions. As an example, efficiency and temperature measurements of the experimental CDR forward-flyback and conventional forward converters at nominal input voltage $V_i = 48$ V and five different output currents are shown in Fig. 9 and Table I, respectively. At light load ($I_o = 10$ A), the CDR forward-flyback converter has a slightly lower efficiency, which is due to a higher core loss and higher clamp-switch loss, as it follows from Table I. At full load ($I_o = 50$ A), a lower secondary copper

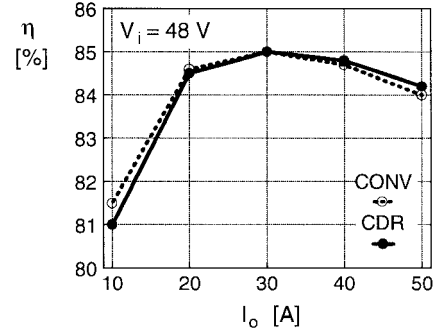


Fig. 9. Efficiency measurements.

TABLE I
TEMPERATURE MEASUREMENTS ($V_i = 48$ V)

I_o [A]	$T(Q_1)$ [°C]		$T(Q_2)$ [°C]		$T(XF_{Fe})$ [°C]		$T(XF_{Cu})$ [°C]	
	CDR	CONV	CDR	CONV	CDR	CONV	CDR	CONV
10	28	28	28	23	34	32	30	30
20	32	32	28	23	38	34	34	34
30	37	36	30	24	41	37	39	39
40	44	42	32	25	45	42	45	48
50	56	52	34	26	51	46	51	56

loss of the CDR forward-flyback converter has the dominant effect, resulting in a slightly higher efficiency of the CDR forward-flyback converter. In fact, the benefits of the ZVS turn on of the CDR forward-flyback converter will become fully advantageous only at higher input voltages as, for example, in off-line applications.

The transformer-secondary copper loss is determined as [9]

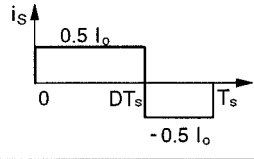
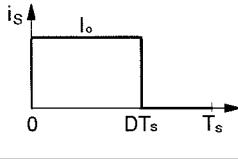
$$P_{Cu,S} = R_{S,dc} I_{S,dc}^2 + \sum_{n=1}^{\infty} R_{S,ac,n} I_{S,ac,n}^2 = R_{S,ac}^{PWM} I_{S,rms}^2 \quad (26)$$

where $R_{S,dc}$ is the dc resistance of the transformer-secondary copper, $R_{S,ac,n}$ is its ac resistance at the n th harmonic of the switching frequency, $R_{S,ac}^{PWM}$ is the total ac resistance of the transformer-secondary copper carrying a PWM (square-wave) current, $I_{S,dc}$ is the dc component of transformer-secondary current i_S , $I_{S,ac,n}$ is the rms of the n th harmonic of current i_S , and $I_{S,rms}$ is the rms of the total secondary current. The current components of the CDR forward-flyback and conventional forward converters are summarized in Table II. The ac component $I_{S,ac}$ is determined as

$$I_{S,ac}^2 = \sum_{n=1}^{\infty} I_{S,ac,n}^2 = I_{S,rms}^2 - I_{S,dc}^2 \quad (27)$$

It should be noticed that the ac components of i_S in Table II are identical. It should be also noticed that $I_{S,rms}(CDR) < I_{S,rms}(CONV)$ for duty cycles $D > 0.25$; however, for duty cycles $D < 0.25$, $I_{S,rms}(CDR) > I_{S,rms}(CONV)$.

TABLE II
TRANSFORMER-SECONDARY CURRENT COMPONENTS

CONVERTER	CDR FRW-FLY	CONV FRW
i_s waveform		
$I_{s,dc}$	$I_o (D - 0.5)$	$I_o D$
$I_{s,rms}$	$0.5 I_o$	$I_o \sqrt{D}$
$I_{s,ac}$	$I_o \sqrt{D(1-D)}$	$I_o \sqrt{D(1-D)}$

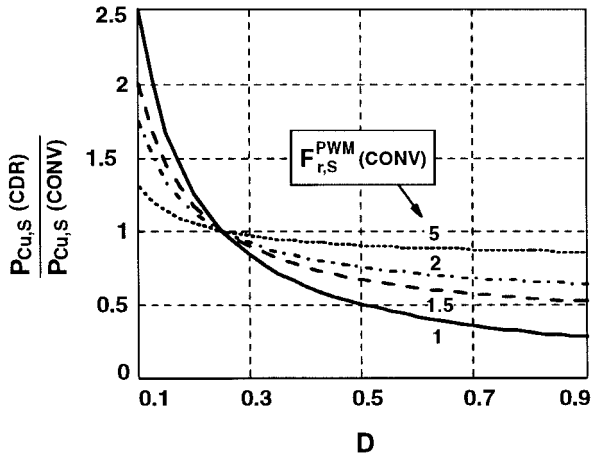


Fig. 10. Ratio of transformer-secondary copper losses of CDR forward-flyback and conventional forward converters.

The ratio of the transformer-secondary copper losses of the CDR forward-flyback and conventional forward converters is obtained as

$$\frac{P_{Cu,s}(\text{CDR})}{P_{Cu,s}(\text{CONV})} = \frac{F_{r,S}^{\text{PWM}}(\text{CONV}) - 1 + \frac{0.25}{D}}{F_{r,S}^{\text{PWM}}(\text{CONV})} \quad (28)$$

where

$$F_{r,S}^{\text{PWM}}(\text{CONV}) = \frac{R_{S,ac}^{\text{PWM}}(\text{CONV})}{R_{S,dc}} \quad (29)$$

is the ratio of the transformer-secondary ac and dc resistances of the conventional forward converter (with unipolar square-wave secondary current). This ratio is determined as [10]

$$F_{r,S}^{\text{PWM}}(\text{CONV}) = D \left[1 + 2 \sum_{n=1}^{\infty} \frac{R_{S,ac,n}}{R_{S,dc}} \cdot \left(\frac{\sin(n\pi D)}{n\pi D} \right)^2 \right]. \quad (30)$$

As can be seen from Fig. 10, the CDR forward-flyback converter has lower transformer-secondary copper losses only

if the ac resistance of the secondary winding is not significantly larger than its dc resistance, i.e., for small values of $F_{r,S}^{\text{PWM}}(\text{CONV})$. For the experimental converter, the calculated value of $F_{r,S}^{\text{PWM}}(\text{CONV})$ at nominal input voltage $V_i = 48$ V ($D = 0.53$) and full load ($I_o = 50$ A) is approximately 1.7, which, from (28), results in a decreased transformer-secondary copper loss of the CDR forward-flyback converter by about 31% compared to that of the conventional forward converter. This is in good agreement with the measurements. As shown in Fig. 10, for duty cycles $D < 0.25$, the CDR forward-flyback converter has higher transformer-secondary copper losses than its conventional counterpart.

VI. SUMMARY

A thorough analysis of the forward-flyback converter with the CDR is performed. To facilitate the understanding of operation, the converter circuit in each topological stage within a switching cycle is reduced to a first- or second-order equivalent circuit. The design of the forward-flyback converter with CDR is illustrated on a 3.3-V/50-A dc/dc converter for the 40–60-V input-voltage range. Advantages and disadvantages of the CDR forward-flyback converter versus the conventional forward converter are theoretically and experimentally evaluated. In particular, the transformer-secondary copper losses are carefully examined. The CDR forward-flyback converter has lower transformer-secondary copper losses than the conventional forward converter only if the ac resistance of the secondary winding is not significantly larger than its dc resistance and if duty cycle $D > 0.25$. For duty cycles $D < 0.25$, the CDR forward-flyback converter has higher transformer-secondary copper losses than its conventional counterpart.

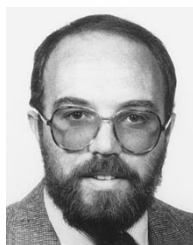
REFERENCES

- [1] A. Cook, *Elements of Electrical Engineering*. New York: Wiley, 1924, pp. 476–478.
- [2] C. Peng, M. Hannigan, and O. Seiersen, “A new efficient high frequency rectifier circuit,” in *Proc. High Frequency Power Conversion (HFPC) Conf.*, June 1991, pp. 236–243.
- [3] K. O’Meara, “A new output rectifier configuration optimized for high frequency operation,” in *Proc. High Frequency Power Conversion (HFPC) Conf.*, June 1991, pp. 219–225.
- [4] L. Balogh, “The performance of the current doubler rectifier with synchronous rectification,” in *Proc. High Frequency Power Conversion (HFPC) Conf.*, May 1995, pp. 216–225.
- [5] N. H. Kutkut, D. M. Divan, and R. W. Gascoigne, “An improved full-bridge zero-voltage switching PWM converter using a two-inductor rectifier,” *IEEE Trans. Ind. Applicat.*, vol. 31, no. 1, pp. 119–126, 1995.
- [6] I. D. Jitaru, “Zero voltage PWM, double ended converter,” in *Proc. High Frequency Power Conversion (HFPC) Conf.*, May 1992, pp. 394–405.
- [7] N. Fröhleke, P. Wallmeier, and H. Grotstollen, “Investigation of active-clamped topologies for low output voltage dc/dc-modules,” in *Proc. High Frequency Power Conversion (HFPC) Conf.*, Sept. 1996, pp. 322–332.
- [8] *Soft Ferrites*, Data Handbook MA01, Philips Components, Eindhoven, The Netherlands, 1996.
- [9] P. S. Venkatraman, “Winding eddy current losses in switch mode power transformers due to rectangular wave currents,” in *Proc. Powercon. 11 Conf.*, 1984, pp. 1–11.
- [10] R. Severns, “A simple, general method for calculating HF winding losses for arbitrary current waveforms,” in *Proc. High Frequency Power Conversion (HFPC) Conf.*, June 1991, pp. 149–159.



Laszlo Huber (M'86) was born in Novi Sad, Yugoslavia, in 1953. He received the Dipl.Eng. degree from the University of Novi Sad, Novi Sad, the M.S. degree from the University of Niš, Niš, Yugoslavia, and the Ph.D. degree from the University of Novi Sad in 1977, 1983, and 1992, respectively, all in electrical engineering.

From 1977 to 1992, he was an Instructor at the Institute for Power and Electronics, University of Novi Sad. In 1992, he joined the Virginia Power Electronics Center at Virginia Tech, Blacksburg, as a Visiting Professor. From 1993 to 1994, he was a Research Scientist at the Virginia Power Electronics Center. Since 1994, he has been a Senior Design Engineer at the Power Electronics Laboratory, Delta Products Corporation, Research Triangle Park, NC, the Advanced R&D unit of Delta Electronics, Inc., Taiwan, one of the world's largest manufacturers of power supplies. His 21-year experience includes the analysis and design of high-frequency, high-power-density, single-phase, and three-phase power processors; modeling, evaluation, and application of high-power semiconductor devices; and modeling, analysis, and design of analog and digital electronics circuits. He has published more than 50 technical papers, holds one U.S. patent, and has two U.S. patents pending.



Milan M. Jovanović (S'86–M'89–SM'89) was born in Belgrade, Yugoslavia. He received the Dipl.Eng. degree in electrical engineering from the University of Belgrade, Belgrade.

Presently, he is the Vice President for Research and Development of Delta Products Corporation, Research Triangle Park, NC—the U.S. subsidiary of Delta Electronics, Inc., Taiwan, one of the world's largest manufacturers of power supplies. His 22-year experience includes the analysis and design of high-frequency high-power-density power processors; modeling, testing, evaluation, and application of high-power semiconductor devices; analysis and design of magnetic devices; and modeling, analysis, and design of analog electronics circuits.